APGC-TDR-62-51

Study of Target Penetration Prediction by High Speed and Ultra High Speed Ballistic Impact

Fourth Quarterly Report

1 April 1962 - 30 June 1962

APGC Technical Documentary Report No. APGC-TDR-62-51

AUGUST 1962   •   Project No. 9860
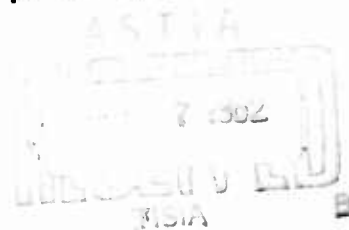
DEPUTY FOR AEROSPACE SYSTEMS TEST

AIR PROVING GROUND CENTER

AIR FORCE SYSTEMS COMMAND • UNITED STATES AIR FORCE

EGLIN AIR FORCE BASE, FLORIDA

FOREWORD

This report was prepared under Air Force Contract Number
AF 08(635)-2155, "Study of Target Penetration Prediction By High
Speed and Ultra High Speed Ballistic Impact". Work was administered
under the direction of APGC (PGTWR), Eglin Air Force Base, Florida,
with Mr. A. G. Bilek as Project Engineer.

ABSTRACT

A statistical analysis of the penetration depth in semi-infinite targets divided by the diameter of the projectile (P_c/D_p) on 1272 experimental shots has been completed. This data was split into 985 low velocity shots and 297 high velocity shots according to the bulk wave velocity in the target material. Separate analyses of the two groups show interesting relationships with existing theoretical and empirical equations.

A semi-rational penetration expression has been developed from a work-energy consideration which suggests that the nonrecoverable target compression and shear strain energies may account for most of the kinetic energy of the projectile. Judging from a preliminary comparison with existing experimental data, a penetration model of the form developed herein shows some promise for predicting impact behavior over a wide velocity range and for different projectile and target materials.

iii

TABLE OF CONTENTS

LIST OF SYMBOLS

A, B	– constants (Eq. 21)
a, b, d, f, h, j, l	– constants
C	– series of constants as C_1, C_2, . . .
c	– dilatational wave velocity
D_p	– projectile diameter
E	– energy
E_p	– impact kinetic energy of projectile
e	– tensile elongation (strain) at fracture (%)
F	– target resistance force
G	– modulus of rigidity
g	– shear strain at fracture (%)
H	– Brinell hardness
K	– bulk modulus
k	– constant
m	– mass
P_c	– crater depth measured from original target surface
p	– pressure
r	– radius
S	– shear strength
T	– target temperature
t	– time
U	– ultimate strength (tensile)
u	– shock velocity

V	- volume
V_c	- crater volume below original target surface
v	- velocity, impact velocity
Y	- yield point or yield strength
γ	- shear strain
ν	- Poisson's ratio
ρ	- mass density
τ	- shear stress

SUBSCRIPTS

B	- backsplash
c	- crater
i	- interface between projectile and target
p	- projectile
pr.	- pressure
S	- denotes material strain, as E_S (strain energy)
t	- target
0	- denotes undisturbed (ahead of shock)
1	- denotes compressed condition (behind shock)
1,2,3. . .	- used with constants

INTRODUCTION

The purpose of this study is to gather and assemble existing data on ballistic impact and on material failure, especially at high impact velocities or large loading - to establish the relative importance of such factors as projectile velocity, mass, projectile-target strengths, ductilities, densities, compressibilities, etc., and to use this information to deduce the mathematical relationships of critical factors as the target structure responds to impact and is penetrated.

Existing experimental data relative to ballistic impact at high velocities are being evaluated on a statistical bases through the use of an RPC 4000 digital computer. The general form of the statistical approach was outlined in the First Quarterly Report [1]. A preliminary analysis of the correlation between depth of penetration and ten independent variables was reported in the Second Quarterly Report [2] and discussed more fully in the Third Quarterly Report [3].

In addition, the general areas of ballistic impact and material failure are being investigated in order to develop relationships which may be tested against existing experimental data. Some general aspects of target behavior under ballistic impact were discussed in the Second Quarterly Report, and some justification was given for the use of static or quasi-static material parameters in the initial statistical analysis. Initial attempts to formulate a theoretical model for the purpose of testing accumulated experimental data were outlined in the Third Quarterly Report. The basis of the theoretical work was the energy conversion processes occurring during impact.

EMPIRICAL MODEL

An analysis of the penetration depth in semi-infinite targets divided by the diameter of the projectile (P_c/D_p) has been completed on 1,270 shots which were reported in enough detail to assign strength parameters to the target materials. The experimental data was divided into two parts: (1) those having impact velocities below v_3 (Hopkins and Kolsky [4]), and (2) those with impact velocities near or above v_3, where

$$v_3 = \sqrt{K_t/\rho_t}$$

The distribution of target materials as a function of impact velocity is given in Figure 1 for the low velocity set (985 shots) and in Figure 2 for the high velocity set (287 shots).
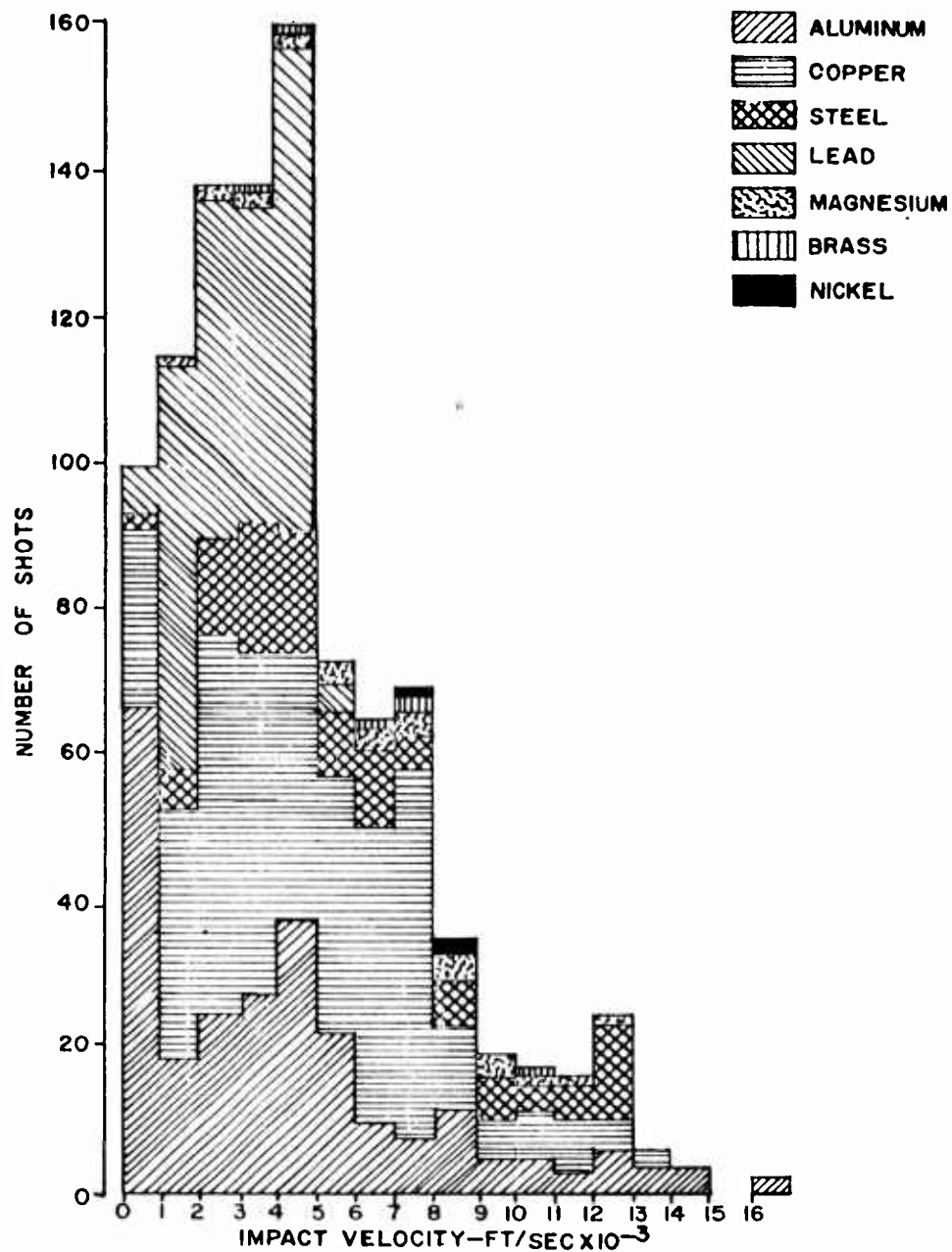
1

Figure 1.   Distribution of Target Materials as a Function
of Velocity - 985 Low Velocity Shots
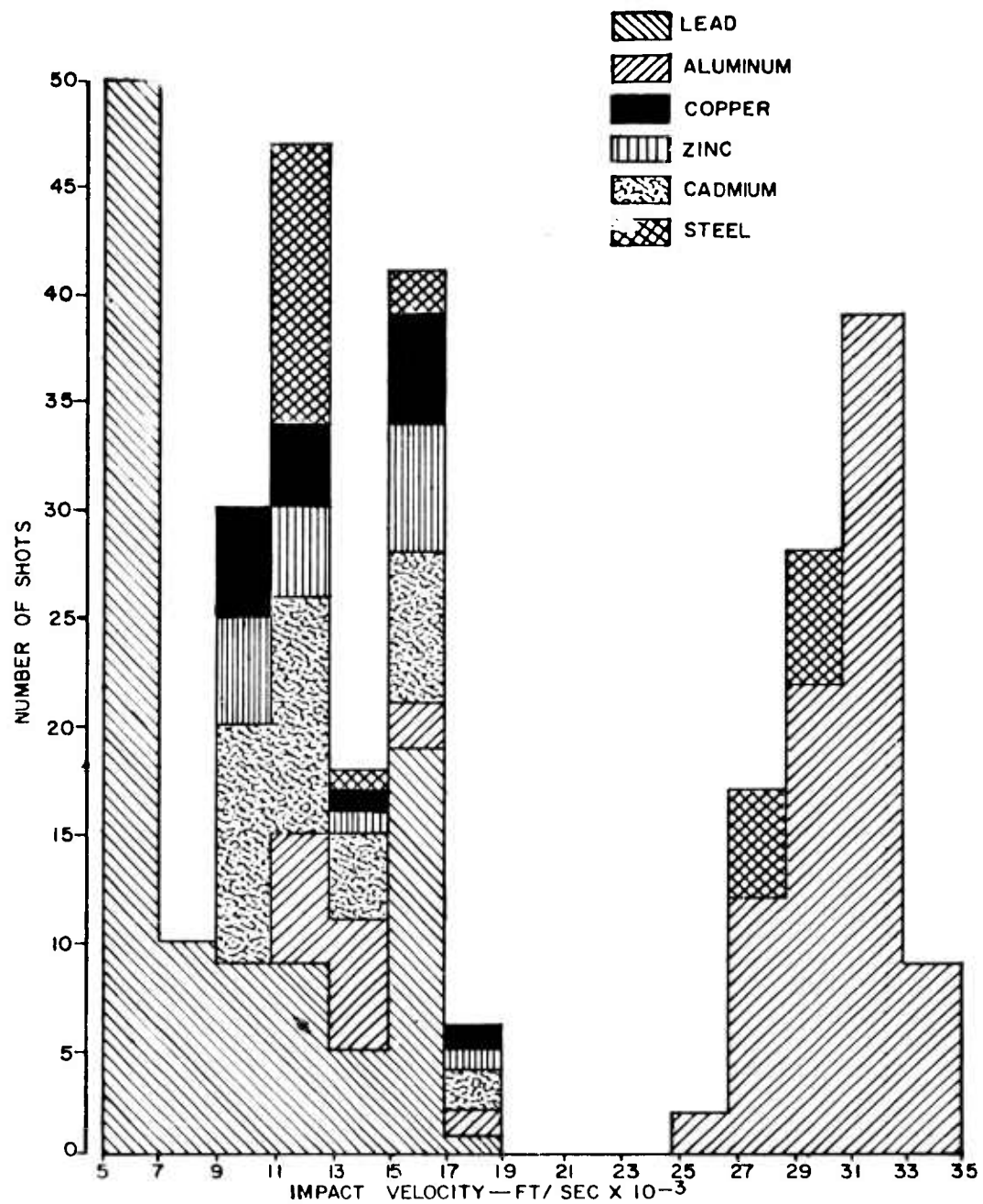
Figure 2.   Distribution of Target Materials as a Function of Velocity -
            297 High Velocity Shots

As was done in the previous analysis of (P_c), reported in the Third Quarterly Report [3], (P_c/D_p) was fitted to a simple power law formula

$$P_c/D_p = k_0 v^{k_1} \rho_t^{k_2} \rho_p^{k_3} \dots \dots$$

with no additional assumptions being made. This equation was then reduced to its associated linear form

$$\log P_c/D_p = \log k_0 + k_1 \log v + k_2 \log \rho_t + \dots \dots$$

and the method of least squares was used to determine a "best" set of values for the variable exponents (coefficients) k_i based on minimizing the value of

$$\sum_{i=0}^{n} \left[\log (P_c/D_p)_{experimental} - \log (P_c/D_p)_{calculated} \right]^2$$

The independent variables were dropped one-by-one, starting with the last, and the effect on the remaining k_i determined. These are summarized in Tables I, II, III and IV for the low velocity data and Tables VI, VII, VIII, IX, X, and XI for the high velocity data.

After the k_i were computed, the usual statistical tests were made to determine the validity of the results. The per cent of variance in log P_c/D_p that is explained by the variation in the logs of the independent variables is given by the multiple correlation coefficients listed in each table. Individual correlation coefficients between all variables were also computed on the low velocity shots. These results appear as Table V.

From Table V, it may be seen that the close correlation between the dilatational wave velocity (c_t), the ultimate strength (U_t), the shear strength (S_t), the Brinell hardness (H_t), and the yield strength (Y_t) render these independent variables statistically indistinguishable. In addition, the correlation coefficient between the bulk modulus (K_t) and each of the above variables is greater than 0.50. Any of the empirical power law equations containing more than one of these closely correlated variables is likely to be completely misleading in the coefficients (exponents) of the correlated variables. All the rest of the variables including the per cent elongation (e_t) were statistically independent.

Although the results of the above analysis have not been thoroughly scrutinized, a few general observations may be made. First, note the startling difference in the multiple correlation of the low velocity and the high velocity data. The best correlation of the high velocity data (49.5%) is little more than half the best correlation of the low velocity data (85%),

4

Table I. The empirical coefficients k_i in the equation

$$P_c/D_p = k_0 \, v^{k_1} \, \rho_t^{k_2} \, \rho_p^{k_3} \, C_t^{k_4} \, I_t^{k_5} \, e_t^{k_6} \, V_p^{k_7}$$

k_0	k_1	k_2	k_3	k_4	k_5	k_6	k_7	Multiple Correlation Coefficient
34.4	1.01	-.578	.969	-1.26	.575	.177	.0229	.829
36.3	.995	-.610	.959	-1.28	.548	.192		.827
173	.963	-.571	.959	-1.35	.613			.823
151	.949	-.515	.988	-1.27				.812
5.45×10^{-3}	.808	.158	.848					.695
7.64×10^{-3}	.649	.283						.532

5

Table II. The empirical coefficients k_i in the equation

$$P_c/D_p = k_0 \, v^{k_1} \, \rho_t^{k_2} \, \rho_p^{k_3} \, H_t^{k_4} \, T_t^{k_5} \, e_t^{k_6} \, V_p^{k_7} \, C_t^{k_8}$$

k_0	k_1	k_2	k_3	k_4	k_5	k_6	k_7	k_8	Multiple Correlation Coefficient
1.21×10^{-3}	1.07	-.294	.951	-.293	.398	.279	.033	.316	.846
0.11×10^{-3}	1.08	-.186	.939	-.366	.329	.320	.036		.845
0.12×10^{-3}	1.06	-.224	.921	-.366	.277	.350			.839
0.46×10^{-3}	.993	-.090	.910	-.380	.363				.825
4.00×10^{-3}	.988	-.078	.932	-.376					.821
5.45×10^{-3}	.808	.158	.848						.695

6

Table III. The empirical coefficients k_i in the equation

$$P_c/D_p = k_o v^{k_1} \rho_t^{k_2} \rho_p^{k_3} S_I^{k_4} T_t^{k_5} e_t^{k_6} v_p^{k_7} C_t^{k_8}$$

k_o	k_1	k_2	k_3	k_4	k_5	k_6	k_7	k_8	Multiple Correlation Coefficients
8.43×10^{-3}	1.06	-.365	.984	-.400	.586	.010	.035	.252	.846
1.99×10^{-3}	1.07	-.298	.983	-.478	.571	-.012	.038		.845
2.19×10^{-3}	1.04	-.338	.963	-.476	.515	.021			.838
2.39×10^{-3}	1.04	-.333	.963	-.480	.522				.838
4.97×10^{-3}	1.03	-.364	.991	-.464					.831
5.45×10^{-3}	.808	.158	.848						.695

7

Table IV. The empirical coefficients k_i in the equation

$$P_c/D_p = k_0 \, v^{k_1} \, \rho_t^{k_2} \, \rho_p^{k_3} \, K_t^{k_4} \, T_t^{k_5} \, e_t^{k_6} \, V_p^{k_7} \, C_t^{k_8}$$

k_0	k_1	k_2	k_3	k_4	k_5	k_6	k_7	k_8	Multiple Correlation Coefficient
1.95	1.01	-.564	.970	-.019	.575	.169	.022	-1.23	.829
.634	.935	.028	.993	-.510	.405	.067	.014		.790
.803	.927	.015	.928	-.523	.391	.069			.789
1.40	.917	.039	.929	-.544	.414				.788
13.4	.910	.052	.952	-.531					.783
5.45×10^{-3}	.808	.158	.848						.695

8

Table V. Individual Correlation Coefficients Between the Variables Used In the Present Analysis

	P_c/D_p	v	ρ_t	ρ_p	T_t	C_t	U_t	Y_t	S_t	e_t	H_t	V_p	K_t
P_c/D_p	.	.055	.024	.053	.024	-.064	-.067	-.064	-.063	.006	-.065	.089	-.054
v			.096	-.238	-.063	.082	.238	.319	.218	.013	.241	-.204	.127
ρ_t				.142	.088	.672	-.343	-.221	-.473	.046	-.268	-.211	-.118
ρ_p					.168	-.013	.017	-.018	-.004	.019	-.016	-.095	.059
T						.078	.053	6.004	.067	.004	.026	-.116	.080
C_t						.	.855	.769	.897	-.025	.791	.011	.535
U_t								.971	.943	-.010	.973	.036	.603
Y_t									.884	-.005	.969	-.045	.579
S_t										-.027	.891	.002	.622
e_t											-.004	-.007	-.006
H_t												.015	.557
V_p													-.120

9

Table VI. High Velocity Data Evaluation of the Coefficients k_i in the Equation

$$P_c/D_p = k_0 v^{k_1} \rho_t^{k_2} \rho_p^{k_3} C_t^{k_4} T_t^{k_5} e_t^{k_6} v_p^{k_7}$$

k_0	k_1	k_2	k_3	k_4	k_5	k_6	k_7	Multiple Correlation Coefficient
.894	.584	-.289	.423	-.694	.238	.304	.014	.440
1.105	.560	-.292	.417	-.698	.232	.304		.439
10.06	.605	-.206	.388	-.793	.105			.419
17.67	.601	-.205	.392	-.785				.418
.470	.250	-.056	.482					.276
1.912	.240	-.144						.034

Table VII. High Velocity Data Evaluation of the Coefficients k_i in the Equation

$$P_c/D_p = k_0 v^{k_1} \rho_t^{k_2} \rho_p^{k_3} H_t^{k_4} I_t^{k_5} e_t^{k_6} V_p^{k_7} C_t^{k_8}$$

k_0	k_1	k_2	k_3	k_4	k_5	k_6	k_7	k_8	Multiple Correlation Coefficient
.481	.591	-.271	.420	-.274	.235	.287	.015	-.614	.440
.0045	.620	-.139	.409	-.224	.202	.175	.017		.436
.0057	.589	-.142	.402	-.225	.193	.175			.434
.0107	.633	-.085	.381	-.253	.131				.428
.0236	.628	-.086	.386	-.249					.427
.470	.250	-.056	.482						.276

11

Table VIII. High Velocity Data Evaluation of the Coefficients k_i in the Equation

$$P_c/D_p = k_0 v^{k_1} \, \rho_t^{k_2} \, \rho_p^{k_3} \, S_t^{k_4} \, T_t^{k_5} \, e_t^{k_6} \, V_p^{k_7} \, C_t^{k_8}$$

k_0	k_1	k_2	k_3	k_4	k_5	k_6	k_7	k_8	Multiple Correlation Coefficient
.304	.603	-.236	.416	-.071	.226	.260	.016	-.497	.440
.020	.625	-.110	.408	-.233	.191	.172	.019		.437
.026	.591	-.113	.401	-.233	.182	.173			.434
.058	.634	-.054	.380	-.262	.120				.429
.118	.630	-.055	.384	-.259					.428
.470	.250	-.056	.482						.276

12

Table IX. High Velocity Data Evaluation of the Coefficients k_i in the Equation

$$P_c/D_p = k_o v^{k_1} \rho_t^{k_2} \rho_p^{k_3} Y_t^{k_4} T_t^{k_5} e_t^{k_6} v_p^{k_7} C_t^{k_8}$$

k_o	k_1	k_2	k_3	k_4	k_5	k_6	k_7	k_8	Multiple Correlation Coefficient
169	.509	-.509	.453	.226	.259	.500	.012	-1.504	.449
.012	.584	-.120	.418	-.160	.210	.197	.017		.419
.015	.555	-.123	.412	-.161	.202	.196			.417
.033	.607	-.056	.387	-.187	.136				.410
.074	.610	-.057	.392	-.184					.409
.470	.250	-.056	.482						.276

13

Table X. High Velocity Data Evaluation of the Coefficients k_i in the Equation

$$F_c/D_p = k_0 v^{k_1} \rho_t^{k_2} \rho_p^{k_3} U_t^{k_4} T_t^{k_5} e_t^{k_6} v_p^{k_7} C_t^{k_8}$$

k_0	k_1	k_2	k_3	k_4	k_5	k_6	k_7	k_8	Multiple Correlation Coefficient
175	.495	-.559	.471	.249	.251	.440	.015	-1.506	.451
.012	.585	-.089	.409	-.170	.214	.246	.015		.416
.015	.560	-.091	.403	-.172	.207	.245			.415
.403	.620	-.002	.371	-.204	.119				.403
.402	.615	-.0001	.375	-.201					.402
.276	.250	-.056	.482						.276

14

Table XI. High Velocity Data Evaluation of the Coefficients k_i in the Equation

$$P_c/D_p = k_o v^{k_1} \rho_t^{k_2} \rho_p^{k_3} K_t^{k_4} I_t^{k_5} e_t^{k_6} V_p^{k_7} C_t^{k_8}$$

k_o	k_1	k_2	k_3	k_4	k_5	k_6	k_7	k_8	Multiple Correlation Coefficient
163	.397	-.406	.555	-.475	.268	.110	.007	-.201	.495
213	.314	-.412	.594	-.553	.259	.108	.007		.492
240	.302	-.414	.592	-.555	.256	.106			.491
658	.306	-.395	.591	-.585	.219				.490
193	.305	-.390	.594	-.573					.487
.470	.250	-.558	.482						.276

in spite of the fact that the high and the low velocity distributions are not as widely separated as one would like. It should be noted that the high velocity correlation has not been completely checked for errors which could considerably alter the correlation coefficients.

It is interesting to note that as long as five or six of the independent variables are used in the empirical formula with the low velocity data, (P_c/D_p) or (P_c) [3] appears to be a function of the first power of the impact velocity. This linear dependence of (P_c) on (v) agrees with the discussion of the simple power law

$$P_c = k\, v^{n} \tag{1}$$

by Herrmann and Jones [5] in which they find that the experimental data, at least for aluminum, fits $n = 1$ over the approximate velocity of 7500 - 12,000 feet/second. They also point out that in the velocity range of 10,000 - 20,000 feet/second penetration may be approximated by Eq. (1) with $n = 2/3$, and from 30,000 - 200,000 it may be approximated by Eq. (1) with $n = 1/3$. Tables VI - X indicate that the high velocity penetration data used in the present empirical analysis is indeed best fit by a power of velocity slightly less than $2/3$. For some unexplained reason, Table XI seems to indicate a dependence on a power of velocity nearer to $1/3$ than $2/3$.

The low velocity data also seem to indicate a dependence of (P_c/D_p) on the first power of the projectile density (ρ_p). This coupled with the linear dependence on velocity mentioned above fits Herrmann and Jones assumption of a resistive force dependent on velocity as

$$F = k\, D_p^{2}\, v$$

which leads to a penetration expression of the form

$$\frac{P_c}{D_p} = k\, \rho_p\, v \tag{2}$$

where k is a constant. As they point out, an equation somewhat like Eq.(2) can be used to fit low-velocity impact data.

The high-velocity data show a dependence of (P_c/D_p) on (ρ_p) to a power slightly greater than $1/3$. This coupled with the dependence on the $2/3$ power of velocity is in agreement with the widely used empirical expression

16

$$\frac{P_c}{D_p} = k \, \rho_p^{1/3} \, v^{2/3} \tag{3}$$

which is obtained for the case where the crater volume is proportioned to the energy and the craters are hemispherical in shape. The fact that Palmer [6] finds the Utah data fits an equation similar to Eq. (3), but with the exponent of (ρ_p) as $\frac{1}{2}$, is also understandable on the basis of the high velocity data, especially in Table XI.

Both the high and low velocity data indicate a real dependence on at least one target strength parameter (c_t and K_t, also being classed as strength parameters because of their close correlation with the strength parameters). The low velocity data seems to favor a dependence of penetration on Brinell hardness to the -1/3 power (Table II), which agrees with Herrmann and Jones [5], and Palmer [6], or on shear strength or bulk modulus to a power of about $-\frac{1}{2}$ (Tables III and IV). The high velocity data (Tables VII - XI) shows a dependence of penetration on Brinell hardness, shear strength, yield strength, or ultimate strength to a power of about -0.2, or on the bulk modulus to a power of about $-\frac{1}{4}$.

The role of the target density is clearly not well defined. A possible reason for this is given in the discussion of the theoretical model. The target temperature coefficients are not considered particularly significant since the shots in which temperature was varied represent such a small percentage of the total.

THEORETICAL MODEL

GENERAL

The study of the transformation processes involved in the dissipation of impact kinetic energy in a hypervelocity ballistic impact is being continued. A semi-rational penetration expression has been developed from a work-energy consideration which suggests that the nonrecoverable target compression and shear strain energies may account for most of the kinetic energy of the projectile. This approach is not intended to delineate the relative importance of the mechanisms of cavitation, shear, plastic flow, etc., but rather to indicate that the resulting cavity formation is a function of certain resistance parameters which appear to be primarily density, compressibility and shear toughness of the target material for a given set of impact conditions. This estimate of the situation is intended to refer primarily to the more ductile targets (as most of the experimental targets have been - - aluminum, steel, copper, lead, etc.), although material shear toughness does provide a measure of relative ductility or brittleness.

17

The kinetic energy of a projectile can be considered as its capacity to do work as a result of its velocity. From the principle of work and kinetic energy, it can be said that the total work done by a projectile on a target is equal to the change in kinetic energy of the projectile, since the negative work done by the target on the projectile should be equal numerically to the positive work done by the projectile on the target. Thus, the impact kinetic energy should be equal to the net positive work done on the target.

The actual work done in moving the crater material backwards is negligible compared with the work required to fracture or dissociate this material from the target. Any recrystallization that takes place is a result of internal deformation accompanied by heat. It appears that the net work done on the target may be determined largely by the nonrecoverable or permanent deformational energy absorbed by the target material. That is to say; the energies dissipated as heat, sound, electromagnetic radiation, etc., are essentially a result of material deformation (accompanied by fric-. tional effects, etc.) and that the permanent deformation itself constitutes the primary work done by the projectile. It is realized that many uncertain-ties such as energy going into shock-wave formation and crack propagation in brittle materials, extent of inelastic deformation into the target, etc,; are involved, although these features are, at least in part, a function of the target's ability to absorb strain energy. Of course, there are bound to be other considerations, such as movement of the entire target, etc., which are assumed to be secondary in this treatment.

The material deformation itself seems to refer to the primary work being done on the target, and the corresponding deformational energy absorbed is dissipated through the different processes. It is thus be-lieved that the correlation of impact kinetic energy with either mechanical deformational work or the combined mechanical, chemical, acoustical, thermal, electrical, etc., energies of dissipation provides dual methods for analyzing the impact problem. In the latter approach the target strain energy absorbed and any work or energy required to recrystallize part of the target should not be combined with the sum total of the backsplash, heat, sound, radiation, etc., energies eventually lost from the target. In connection with the recrystallization process, the work or energy required to recrystallize the grains might be considered a part of the deformational work being done on the target. Presumably, this effect could be included in the general defor-mational parameters chosen.

The problem of bridging the gap between lower velocity and hypervelocity ballistic impact theory requires an explanation of how the projectile moving into a target with an initial velocity greater than that of any stress wave that can be detached affects the cratering process. One point that seems evident, however, is that in both cases, the cratering process depends largely upon the target's ability to absorb energy which must be related in some way to pertinent impact and material parameters. If the relations governing the

18

pressures developed in subsonic and hypervelocity impacts constitute the
primary difference in the two cases, it is shown in the discussion of
Eqs. (10, (19), (27), and (63) that the subsonic pressures, determined
from the Bernoulli relation (Eq.(10)) and the hypervelocity shock pressures,
determined from one-dimensional shock theory (Eq. (19)), yield similar pene-
tration expressions in all but possibly extremely high velocity impacts.

It is suggested that, in general, parameters which provide a measure
of a target's ability to "stop" a projectile (and in doing so to describe
the cratering process) are appropriate compression and shear energy ab-
sorbing parameters. The energy absorbed in direct compression and the
shear energy absorbed primarily in the cratering process no doubt take
on varying degrees of importance, depending on target material, impact
velocity, etc. There are, of course, discrepancies involved in the use
of static or low strain-rate material properties, but these difficulties
are presently unavoidable regardless of the method of analysis. It does
appear that the pertinent static material properties are, generally speak-
ing, indicative of the behavior under conditions of high pressure, high
strain rates, etc. That is, higher pressures generally produce greater
strengths and ductilities (at least shear ductility) but less compressibil-
ity, etc., and higher strain rates generally produce greater strengths,
but less compressibility and ductility, etc.

In order to study the behavior of the target during the impact process,
it is necessary to consider the nature of the loading and the state of the
material. The ordinary use of the terms solid and fluid seem to be insuf-
ficient in describing the target material under such high strain rates and
pressures, etc. The hydrodynamic theory assumes that the target material
has been stressed far beyond its strength and therefore behaves as a liquid
with virtually no shear strength. However, since extremely high pressures
tend to congeal liquids, the high pressures produced during impact may be
simply a result of the quasi-solid target material's ability to develop
such high pressures. Also, high pressures are known to substantially in-
crease shear strengths so that, even though some type of material flow un-
doubtedly takes place, the shear strain energy absorbed may be a significant
factor. Regardless of the magnitude of the impact velocity, there must be
a certain period at the end of the crater formation period in which material
strength plays a dominant role.

The compression and shear strain energy absorbed in the impact process
depend generally on the following factors:

1. The magnitude and distribution of the pressures that
the target material develops under the impact conditions along with
the rate at which the high initial pressures are attenuated.

2. The compressibility of the target material or its
reciprocal, the ability of the material to resist compressive
deformation.

19

3. The shear toughness of the target material under
the impact conditions.

DEVELOPMENT OF MODEL

The general expressions for compression and shear strain energy ab-
sorbed for the case of a simplified hemispherical surface are:

Compression Strain Energy
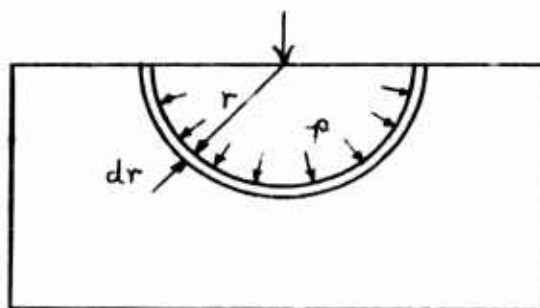
$$(E_s)_{pr} = 2\pi \int p \left(\frac{\Delta V}{V}\right) r^2 \, dr \tag{4}$$

Shear Strain Energy

$$(E_s)_{\tau} = 2\pi \int \tau \gamma \, r^2 \, dr \tag{5}$$

20
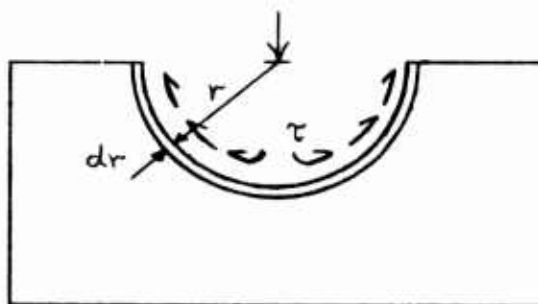
As soon as the impacting materials begin to deform, the maximum developable pressure might be considered as the dynamic fluid pressure (or stagnation pressure) for the smaller density material.

$$p = C_1 (\rho v^2) \tag{6}$$

where C_1 is a constant and ρ is the smaller of the projectile or target material density.

However, a better estimate of the pressure developed might be obtained for the case in which both projectile and target are regarded as incompressible fluids. In this case, from the Bernoulli relation,

$$p = \frac{1}{2} \rho_t v_i^2 = \frac{1}{2} \rho_p (v - v_i)^2 \tag{7}$$

where v = impact velocity
       v_i = velocity of projectile-target interface

From Eq. (7),

$$(v - v_i) = \frac{\sqrt{\rho_t}}{\sqrt{\rho_p}} v_i \tag{8}$$

or

$$v_i = \frac{\sqrt{\rho_p}}{\sqrt{\rho_p} + \sqrt{\rho_t}} v \tag{9}$$

Hence,

$$p = \frac{1}{2} \rho_t v_i^2 = C_2 \frac{\rho_p \rho_t}{(\sqrt{\rho_p} + \sqrt{\rho_t})^2} v^2 \tag{10}$$

or

$$p = C_2 \rho_{p-t} v^2 \tag{11}$$

where C_2 is a constant and ρ_{p-t} refers to a composite projectile-target density term defined as

$$\rho_{p-t} = \frac{\rho_p \rho_t}{(\sqrt{\rho_p} + \sqrt{\rho_t})^2} \tag{12}$$

21

Interesting comparisons are made on Lines 5 and 6 of Table XII which show the variation of the composite density term with the projectile and target densities. Note that when the projectile and target densities are equal, the composite density term is 0.25 times either one.

Alternately, the initial contact pressure might be determined by one-dimensional shock theory. The conservation of mass and momentum equations are written for a stationary shock front, where the undisturbed condition (ahead of the shock) and the compressed condition (behind the shock) are denoted by the subscripts 0 and 1, respectively.

Conservation of Mass $\qquad \rho_1 (u - v_1) = \rho_0 (u - v_0)$

$$(13)$$

Conservation of Momentum $\qquad (p_1 - p_0) = \rho_0 (u - v_0)(v_1 - v_0)$

where u is the shock velocity and v is the particle velocity.

Solving Eq. (13) yields

$$u = v_0 \pm \sqrt{\frac{\rho_1}{\rho_0} \frac{(p_1 - p_0)}{(\rho_1 - \rho_0)}} \qquad (14)$$

and

$$v_1 = v_0 \pm \sqrt{\frac{(p_1 - p_0)(\rho_1 - \rho_0)}{\rho_1 \rho_0}} \qquad (15)$$

22

Table XII. Miscellaneous Calculations

Steel Projectile* - Target Material →	4140 Steel	Copper	Zinc	Magn.	Alum.	Lead	Reference
1. From "best fit" curves (Utah, p.14) $\frac{V_c}{E_p}$	0.20×10^{-10} cm³/dyne-cm	0.60	0.65	0.84	1.67	4.25	Utah [7]
2. (Line 1.) x (0.88 x 10^10 dyne-cm) = V_c*	0.176 cm³	0.53	0.57	0.74	1.47	3.74	Calculated
3. ρ_t	7.90 gm/cm³	8.95	7.14	1.74	2.70	11.4	Physics Handbook [8]
4. (See Eq. 12) $\rho_{p-t} = \rho_p A (\sqrt{\rho_p} + \sqrt{\rho_t})^2$	1.96 gm/cm³	2.11	1.86	0.766	1.07	2.33	Calculated
5. ρ_{p-t}/ρ_t = (Line 4.)/ρ_t	0.25 dimensionless	0.24	0.26	0.44	0.40	0.20	Calculated
6. ρ_{p-t}/ρ_p = (Line 4.)/ρ_p	0.25 dimensionless	0.27	0.24	0.10	0.14	0.30	Calculated
7. (The steel value was given for iron, but value also good for steel) K_t	1.67×10^{12} dyne/cm²	1.33	0.57	0.34	0.75	0.44	Kent Handbook [9]
8. Compressibility: $1/$(Line 7.) = $1/K_t$	0.600×10^{-12} cm²/dyne	0.752	1.76	2.94	1.33	2.28	Calculated
9. (Line 8.) x (980) = $1/k_t$	0.589×10^{-9} cm²/gm	0.737	1.722	2.89	1.305	2.23	Calculated
10. [Parameters for Eq. (21),] A_t	0.584×10^{-9} cm²/gm	0.732			1.334	2.37	Nadai, [10]
11. [$\frac{\Delta V}{V} = Ap - Bp^2$] B_t	0.040×10^{-17} cm⁴/gm²	0.27			0.35	1.73	Rinehart & Pearson [11]
12. S_t	55.0×10^8 dyne/cm²	15.8	13.1	13.0	6.5	1.2	Utah [1]
13. Values for q could not be found. Tensile elongation values were used. Both provide a relative measure of ductility. q_t	0.17 dimensionless	0.20	0.15	0.16	0.12	0.30	Metals Handbook [12] (Except ANC-5 for Steel) [13]
Calculations:							
14. $\frac{V_c}{E_p} \frac{1}{k_t} \rho_{p-t}^2 v^4$	0.074 dimensionless	0.322	0.633	0.233	0.406	8.419	
15. $\frac{V_c}{E_p} S_t$	0.1100 dimensionless	0.0948	0.0852	0.1092	0.1086	0.0510	
16. $\frac{V_c}{E_p} (Sq)_t$	0.0187 dimensionless	0.0190	0.0128	0.0175	0.0130	0.0153	
17. (See Eq.30), Const. = $\frac{1}{\frac{V_c}{E_p} S_t}$	9.1 dimensionless	10.5	11.7	9.1	9.2	19.6	70% ⊕
18. (See Eq.31), Const. = $\frac{1}{\frac{V_c}{E_p}(Sq)_t}$	5.4 dimensionless	5.3	7.8	5.7	7.7	6.5	22% ⊕

*For $\rho_p = 7.80$ gm/cm³, $V_p = 0.0564$ cm³, $v = 2$ Km/sec : $E_p = \frac{1}{2}\rho_p V_p v^2 = 0.88 \times 10^{10}$ dyne-cm

⊕ Maximum Deviation From Mean Value.

If the change in compressibility with pressure is neglected (equivalent to neglecting the nonlinear term in Eq. (21)), the shock velocity u can be taken as the dilatational wave velocity, or

$$u = c \tag{16}$$

The appropriate expression for the dilatational wave velocity c for the case where the compressibility behavior is assumed to be linear and where the contribution of shear stiffness G is neglected (inelastic range) is

$$c = \sqrt{\frac{K}{\rho}}$$

Solving Eqs. (14), (15) and (16), following the assumption that $v_0 = 0$ and $p_0 = 0$ (corresponding to the initial impact condition) yields,

for the target
$$p_1 = v_1 c_t \rho_t \tag{17}$$

and for the projectile
$$p_1 = (v - v_1) c_p \rho_p \tag{18}$$

where unsubscripted v is impact velocity. Eliminating v_1 between Eqs. (17) and (18) yields an expression for the initial interface pressure

$$p_1 = \frac{c_p \rho_p \, c_t \rho_t}{c_p \rho_p + c_t \rho_t} v \tag{19}$$

A comparison of the Bernoulli pressure (Eq. (10)) with the shock pressure (Eq. (19)) in the Discussion Section shows that similar penetration expressions are obtained in all but possibly extremely high velocity impacts.

The factors that govern the rate at which the initial pressures are attenuated are not known. Also, the distribution of pressure around the crater rim at a given instant is unknown. However, a representative pressure variable might be considered to be a function of the initial

24

pressure p. Although the extent of the inelastic deformation in the target is uncertain, it would appear to be generally a function of the target's ability to absorb compression energy. Thus, the upper limit for the integral (Eq. (4)) might be considered as some function of the crater depth (constant times crater depth P_c for linear function). Assuming this function to be linear, a solution for Eq. (4) would be

$$\left(E_s \right)_{pr.} = C_3 \, p \left(\frac{\Delta V}{V} \right)_t \, P_c^3 \qquad (20)$$

where C_3 is a constant.

A measure of the unit volume change of the target material, $\frac{\Delta V}{V}$, might be taken from hydrostatic compressibility data which has been obtained for a few materials. An expression of the form

$$\frac{\Delta V}{V} = A_p - B_p^2 \qquad (21)$$

seems to fit these curves fairly well, where A and B are constants. Actually, the hugoniot relationship developed for a given equation of state could be used here, although this would hardly seem consistent with the use of static or low strain-rate strength parameters (especially when the strength effect is considerable).

It can be noted in Table XII that the factor A in Eq. (21) and the compressibility 1/K (reciprocal of bulk modulus) are almost identical and that the factor B varies similarly between materials. If the non-linear term in Eq. (21) is discarded, this equation can be taken as

$$\frac{\Delta V}{V} = \frac{1}{K} \, p \qquad (22)$$

Considering the shear toughness of the crater material to be the product of S and g and the plastic shear strain in the vicinity of the final crater boundary to be a function of this toughness factor; also assuming the extent of the inelastic shear strain into the target to be some linear function of the crater depth, a solution of Eq. (5) is

$$\left(E_s \right)_{\tau} = C_4 \, \left(S_g \right)_t \, P_c^3 \qquad (23)$$

where C_4 is a constant.

25

Equating the impact kinetic energy to the sum of the two work or energy expressions, Eqs. (20) and (23), yields

$$E_p = \frac{1}{2} \rho_p V_p v^2 = P_c^3 \left[C_3 \, p \left(\frac{\Delta V}{V} \right)_t + C_4 (S_g)_t \right] \quad (24)$$

or

$$\frac{V_c}{E_p} = \frac{1}{C_5 \, p \left(\frac{\Delta V}{V} \right)_t + C_6 (S_g)_t} \quad (25)$$

where C_5 and C_6 are new constants, since $V_c = \frac{2}{3} \pi P_c^3$ for the hemispherical crater. Substituting Eqs. (11) and (22) into Eq. (25) yields

$$\frac{V_c}{E_p} = \frac{1}{a_1 \frac{1}{K_t} \rho_{p-t}^2 v^4 + a_2 (S_g)_t} \quad (26)$$

which will be used to investigate the Utah data [7]. Also substituting Eqs. (11) and (22) into Eq. (24) yields

$$\frac{P_c}{V_p^{1/3}} = \frac{\rho_p^{1/3}}{\left[a_3 \frac{1}{K_t} \rho_{p-t}^2 v^2 + a_4 (S_g)_t v^{-2} \right]^{1/3}} \quad (27)$$

The use of Eq. (21) instead of Eq. (22) in obtaining Eqs. (26) and (27) leads, respectively, to

$$\frac{V_c}{E_p} = \frac{1}{C_5 A_t \rho_{p-t}^2 v^4 - C_5 B_t \rho_{p-t}^3 v^6 + C_6 (S_g)_t} \quad (28)$$

26

and

$$\frac{P_c}{V_p^{1/3}} = \frac{\rho_p^{1/3}}{\left[C_7 A_t \rho_{p\text{-}t}^2 \, v^2 - C_7 B_t \rho_{p\text{-}t}^3 \, v^4 + C_8 (S_g)_t \, v^{-2}\right]^{1/3}} (29)$$

The Utah data [7] will now be used to study the proposed penetration equation in the form of Eq. (26).

$$\frac{V_c}{E_p} = \frac{1}{a_1 \frac{1}{K_t} \rho_{p\text{-}t}^2 \, v^4 + a_2 (S_g)_t} \qquad (26)$$

This form of the equation involving the simpler compression energy expression (employing Eq. (22) instead of Eq. (21)) is used in estimating the relative effects of compressibility and shear toughness. The various values are shown in Table XII along with appropriate reference comments. One shortcoming (noted on Line 13 of Table XII) is the necessity of using tensile elongation values instead of ultimate shear strains g . This is not too unreasonable, however, since both provide a relative measure of ductility. The ultimate shear strains for the different target materials could not be found.

The Utah report [7] showed an approximate correlation of volume/energy with shear strength S_t (Eq. (30)) for all target materials tested except lead.

$$\frac{V_c}{E_p} = \frac{1}{Const. \, (S)_t} \qquad (30)$$

These constants are repeated on Line 17 of Table XII where maximum deviation from the mean value is 70%. Since lead is the most ductile material of the group, the possibility of a closer correlation of volume/energy with shear toughness is suggested as

$$\frac{V_c}{E_p} = \frac{1}{Const. \, (S_g)_t} \qquad (31)$$

These constants are shown on Line 18 of Table XII where the maximum deviation from the mean value is only 22%, using the tensile elongation

27

parameters for the ultimate shear strain g_t.

Rewriting Eq. (26),

$$\frac{V_c}{E_p} \frac{1}{K_t} \rho_{p-t}^2 v^4 a_1 + \frac{V_c}{E_p} (S_g)_t a_2 = 1 \tag{32}$$

or, referring to Table XII,

$$(\text{line } 14) \, a_1 \quad + \quad (\text{line } 16) \, a_2 = 1 \tag{33}$$

Approximate values of $a_1 = 0.02$ and $a_2 = 60$ were found by iteration using the Utah data. When substituted into Eq. (33), these constants yield a maximum deviation from the mean of 20% for the different materials, as shown below.

$$
\begin{aligned}
\text{steel:} &\quad .074 \, a_1 + 0.0187 \, a_2 \cong 1.1 \\
\text{copper:} &\quad .322 \, a_1 + .0190 \, a_2 \cong 1.1 \\
\text{zinc:} &\quad .633 \, a_1 + .0128 \, a_2 \cong 0.8 \\
\text{magnesium:} &\quad .233 \, a_1 + .0175 \, a_2 \cong 1.1 \\
\text{aluminum:} &\quad .406 \, a_1 + .0130 \, a_2 \cong 0.8 \\
\text{lead:} &\quad 8.419 \, a_1 + .0153 \, a_2 \cong 1.1
\end{aligned}
\tag{34}
$$

It is interesting to note in the above relations that the very much higher coefficient of a_1 for lead may indicate the relative importance of the density term when the impact velocity is in the vicinity of the target dilatational wave velocity (the case only for lead here). The maximum impact velocities were about 2 km/sec.

OTHER MODELS

This section is adapted from the excellent paper by Herrmann and Jones [5] for purposes of comparison and discussion. By referring to an arbitrary target resistance force F, the work-kinetic energy expression can be written as

$$\rho_p V_p v \, dv = -F \, dP_c \tag{35}$$

which can be integrated to yield a penetration expression for a given definition of F. This approach, however, does not intuitively include any work done on the target in the form of shear deformation.

Virtually any power expression of the form

$$\frac{P_c}{V_p^{1/3}} = C \rho_p^b v^d \tag{36}$$

can be obtained from Eq. (35) by assuming the resistance force to be of the form

$$F = C_1 \left(P_c^f, V_p^h, \rho_p^{\dot{j}}, v^l \right) \tag{37}$$

where $l \neq -2$ ($l = -2$ yields a logarithmic relation). For example, if the resistance force is assumed to be proportional to penetration, as

$$F = C_2 P_c^2 \tag{38}$$

or proportional to all four parameters, as

$$F = C_3 \frac{P_c^5}{V_p \rho_p v^2} \tag{39}$$

Eq. (35) reduces in both cases to

$$\frac{P_c}{V_p^{1/3}} = C_4 \rho_p^{1/3} v^{2/3} \tag{40}$$

when the constant of integration is assumed zero.

If C_4 is defined as some target material strength parameter, one possibility that provides an approximate data fit is

$$C_4 = C_5 H_t^{-1/3} \tag{41}$$

where the strength parameter H_t is the Brinell hardness. Eq. (40) then becomes

$$\frac{P_c}{V_p^{1/3}} = C_5 \frac{\rho_p^{1/3} v^{2/3}}{H_t^{1/3}} \tag{42}$$

which can be written as

$$\frac{P_c}{V_p^{1/3}} = C_5 \left(\frac{\rho_p}{\rho_t}\right)^{1/3} \left(\frac{\rho_t v^2}{H_t}\right)^{1/3} \tag{43}$$

Eq. (43) can also be obtained by equating the volume/energy ratio to $H^{-1/3}$ and assuming a hemispherical crater.

A closer fit than Eq. (43) has been found by adjusting the density ratio power as

$$\frac{P_c}{V_p^{1/3}} = a_5 \left(\frac{\rho_p}{\rho_t}\right)^{2/3} \left(\frac{\rho_t v^2}{H_t}\right)^{1/3} \tag{44}$$

This expression involving both density and strength terms was shown by Herrman and Jones to provide the best power function fit for a variety of target and projectile materials (a_5 about 0.36), although still over a somewhat limited range of impact velocities.

If now the resistance force F is assumed to be dependent on the inertia forces exerted by the target,

$$dF = (dm)a = (Area \; ds \; \rho_t) \frac{dv}{dt}$$
$$= C_6 V_p^{2/3} v \; dt \; \rho_t \; \frac{dv}{dt}$$
$$= C_6 V_p^{2/3} \rho_t \; v \; dv \tag{45}$$

30

and

$$F = \frac{1}{2} C_6 V_p^{2/3} \rho_t v^2 \tag{46}$$

which when substituted into Eq. (35) yields upon integration

$$\frac{P_c}{V_p^{1/3}} = C_7 \frac{\rho_p}{\rho_t} \ln v + C_8 \tag{47}$$

If C_8 is interpreted as a material strength parameter, independent of velocity, another expression similar to Eq. (46) might be written as

$$F = C_9 V_p^{2/3} \left(\rho_t v^2 + C_{10} H_t \right) \tag{48}$$

which leads, instead of Eq. (47), to

$$\frac{P_c}{V_p^{1/3}} = \frac{1}{2 C_9} \left(\frac{\rho_p}{\rho_t} \right) \ln \left[\rho_t v^2 + C_{10} H_t \right] + C_{11} \tag{49}$$

Assuming the constant c_{11} to be zero,

$$\frac{P_c}{V_p^{1/3}} = \frac{1}{2 C_9} \left(\frac{\rho_p}{\rho_t} \right) \ln \left[1 + \frac{1}{C_{10}} \left(\frac{\rho_t v^2}{H_t} \right) \right] C_{10} H_t \tag{50}$$

Eq. (50) was written by Herrmann and Jones as

$$\frac{P_c}{V_p^{1/3}} = C_{11} \left(\frac{\rho_p}{\rho_t} \right) \ln \left[1 + \frac{1}{C_{10}} \left(\frac{\rho_t v^2}{H_t} \right) \right] \tag{51}$$

where $C_{10} H_t$ multiplier (a constant for a given material) was deleted. From Eq. (51), a least squares fit of existing experimental data to an equation of the form

$$\frac{P_c}{V_p^{1/3}} = C_{12} \ln \left[1 + \frac{1}{C_{13}} \left(\frac{\rho_t v^2}{H_t} \right) \right] \tag{52}$$

31

determined a more appropriate expression than Eq. (51) to be

$$\frac{P_c}{V_p^{1/3}} = a_6 \left(\frac{\rho_p}{\rho_t} \right)^{1/2} \ln \left[1 + \frac{1}{a_7} \left(\frac{\rho_p}{\rho_t} \right)^{2/3} \left(\frac{\rho_t v^2}{H_t} \right) \right] \qquad (53)$$

which can be approximated by the expression

$$\frac{P_c}{V_p^{1/3}} = C_{14} \left(\frac{\rho_p}{\rho_t} \right)^{0.72} \left(\frac{\rho_t v^2}{H_t} \right)^{1/3} \qquad (54)$$

for a velocity range limited to medium and moderately high impact velocities. Eq. (54) compares very closely with Eq. (44).

The logarithmic expression involving both density and strength terms has been shown by Herrmann and Jones to fit experimental data over the entire experimental range, but only when appropriate values for the constants are used for given target and projectile materials. These constants were found to vary widely between materials.

DISCUSSION

In referring to theoretical, semi-rational or entirely empirical penetration prediction models, one point that must remain clear is that the actual mechanisms involved in the crater formation process in hypervelocity impacts are astronomically complex. Also the use of static or relatively low strain-rate (and low pressure) mechanical properties of the materials renders the problem that much more vague. It can only be hoped that any particular penetration expression providing an engineering approximation includes those factors that have a dominate effect on the cratering process in general.

Specific attention will now be focused on Eqs. (26), (27), (44) and (53).

$$\frac{V_c}{E_p} = \frac{1}{a_1 \frac{1}{K_t} \rho_{p-t}^2 v^4 + a_2 (S_g)_t} \qquad (26)$$

$$\frac{P_c}{V_p^{1/3}} = \frac{\rho_p^{1/3}}{\left[a_3 \frac{1}{K_t} \rho_{p \cdot t}^2 \, v^2 + a_4 \, (S_g)_t \, v^{-2} \right]^{1/3}} \tag{27}$$

$$\frac{P_c}{V_p^{1/3}} = a_5 \left(\frac{\rho_p}{\rho_t} \right)^{2/3} \left(\frac{\rho_t \, v^2}{H_t} \right)^{1/3} \tag{44}$$

$$\frac{P_c}{V_p^{1/3}} = a_6 \left(\frac{\rho_p}{\rho_t} \right)^{1/2} \ln \left[1 + \frac{1}{a_7} \left(\frac{\rho_p}{\rho_t} \right)^{2/3} \left(\frac{\rho_t \, v^2}{H_t} \right) \right] \tag{53}$$

where

$$\rho_{p \cdot t} = \frac{\rho_p \, \rho_t}{\left(\sqrt{\rho_p} + \sqrt{\rho_t} \right)^2} \tag{12}$$

In addition to a projectile density term, Eqs. (27), (44) and (53) all have a target density term, a target strength parameter and the impact velocity variable. Whereas the Brinell hardness was empirically selected in Eqs. (44) and (53), the shear toughness was rationally included in Eq. (27). The form of the density terms vary widely between the different expressions. One point regarding Eq. (27) is that the sum of the density (in the form of compressibility) and shear toughness terms, each with velocity multipliers provide an interesting possibility for explaining behavior over wide velocity ranges. For example, it appears that the empirically determined constants a_3 and a_4 in Eq. (27) would require the density term to be relatively small for lower and medium velocities when fitted to different materials, and that the density term would increase relative to the toughness term as the velocity increases (note the two powers of the velocity variables and the results of Eq. (34)).

A linear volume-energy relationship has been empirically determined for certain ranges of impact data.

33

$$E_p = b + d V_c \tag{55}$$

or

$$\frac{V_c}{E_p} = \frac{1}{b/V_c + d} \tag{56}$$

where b refers to the E_p -intercept and d is the slope.

Eq. (56) has the same form as Eq. (26) where the constant slope d in Eq. (56) corresponds to the constant shear toughness term in Eq. (26). Eq. (56) would, however, only be constant when the b/V_c term was negligible. Actually, the E_p -intercept (or b) is nearly zero for most lower and medium velocity data. This then adds weight to the form of Eq. (26), or its equivalent Eq. (27), where the density term is small for lower and medium velocity ranges. For higher velocity, the constancy of Eq. (56) would no longer be expected and would no longer be provided by Eq. (26).

From an analysis of Eq. (27), the following functions are written for certain limiting conditions:

$$\frac{P_c}{V_p^{1/3}} = \text{a function of } (Sg)_t^{-1/3} \tag{57}$$

$$= \text{a function of } \left[v^2 + v^{-2} \right]^{-1/3} \tag{58}$$

$$= \text{a function of } \frac{\rho_p^{1/3}}{\rho_p^{2/3} \rho_t^{2/3} / \left[\sqrt{\rho_p} + \sqrt{\rho_t} \right]^{4/3}} =$$

$$\text{a function of } \left[\rho_p^{1/3} + \frac{1}{\rho_p^{1/6}} + \frac{1}{\rho_p^{4/6}} - \frac{1}{\rho_p^{7/6}} + \frac{1}{\rho_p^{10/6}} - \cdots \right] , \tag{59}$$

34

a function of $\left[\dfrac{1}{\rho_t{}^{2/3}} + \dfrac{1}{\rho_t{}^{1/6}} + \rho_t{}^{2/6} - \rho_t{}^{5/6} + \rho_t{}^{8/6} - \cdots\right]$ (60)

= a function of $\left(\dfrac{1}{K_t}\right)^{-1/3}$ (61)

If the density term in Eq. (27) is negligible at lower velocities, then Eq. (57) should be approximately correct. The penetration relation with the shear strength to the minus 1/3rd power $S_t{}^{-1/3}$ (Brinell hardness gives approximately the same relation) has been observed in the past. It is shown in Table XII that a closer penetration relation with the shear toughness $(Sg)_t$ results for a certain set of data (actually V_c/E_p proportional to $(Sg)_t$ was shown in Table XII). It is suggested that in empirical correlations the product of S_t and g_t (the shear toughness) rather than the two parameters separately might be expected to provide better data fits.

When the compressibility (density) term is negligible in Eq. (27), Eq. (58) reduces to

$$P_c = a \text{ function of } v^{2/3}$$ (62)

In low and medium velocity impacts the compressibility effect appears to be small, and the 2/3rds power has been found to govern most data. It does appear that in these velocity ranges the shear toughness is the predominate parameter compared to density as evidenced for example by a greater penetration in lead than in steel, where the lead shear toughness is smaller than steel, although the density is larger.

At very high velocities the density term as well as the shear term in the denominator of Eq. (27) would presumably be significant, so that the target penetration varies functionally with the velocity as Eq. (58). This would tend to move the curve of Eq. (62) in the direction of the "hydrodynamic theory" 1/3rd power relation.

With regard to the question of the appropriate power for the projectile density ρ_p, values of $\rho_p{}^{1/3}$ to $\rho_p{}^{2/3}$ or so have been reasonably well established as limits of applicability. For Eqs. (44) and (53) Herrmann and Jones determined values of approximately $\rho_p{}^{2/3}$, while the work of Palmer [6] indicates a value of $\rho_p{}^{1/2}$ to provide the best fit. When the compressibility term is negligible, Eq. (27) yields a penetration expression as a function of $\rho_p{}^{1/3}$. However, as the compressibility

term becomes more important, Eq. (59) indicates the appropriate ρ_p -power to move in the direction of the $\rho_p^{2/3}$ -curve (See Figure 3).

The variation of penetration with target density ρ_t is shown by Eq. (60) for the limiting case where the shear toughness term is small. The first term is $\rho_t^{-2/3}$ which is then adjusted by the other terms in the equation. The reason a ρ_t -term has not always been empirically included in the past could be that the density term is relatively small for the experimental range of velocities, and thus the target density effect is not well defined. The same is true for the compressibility parameter $1/K_t$ given by Eq. (61).

Limit of Eq. (59): $\qquad \rho_p^{1/3} \left[\dfrac{\rho_p^{1/2} + 2 + \dfrac{2}{\rho_p^{1/2}}}{\rho_p^{1/2} + 1} \right]$

Limit of Eq. (64): $\qquad \rho_p^{1/3} \left[\dfrac{\rho_p + 2}{\rho_p + 1} \right]$

Figure 3. $P_c/V_p^{1/3}$ Versus Projectile Density Functions

36
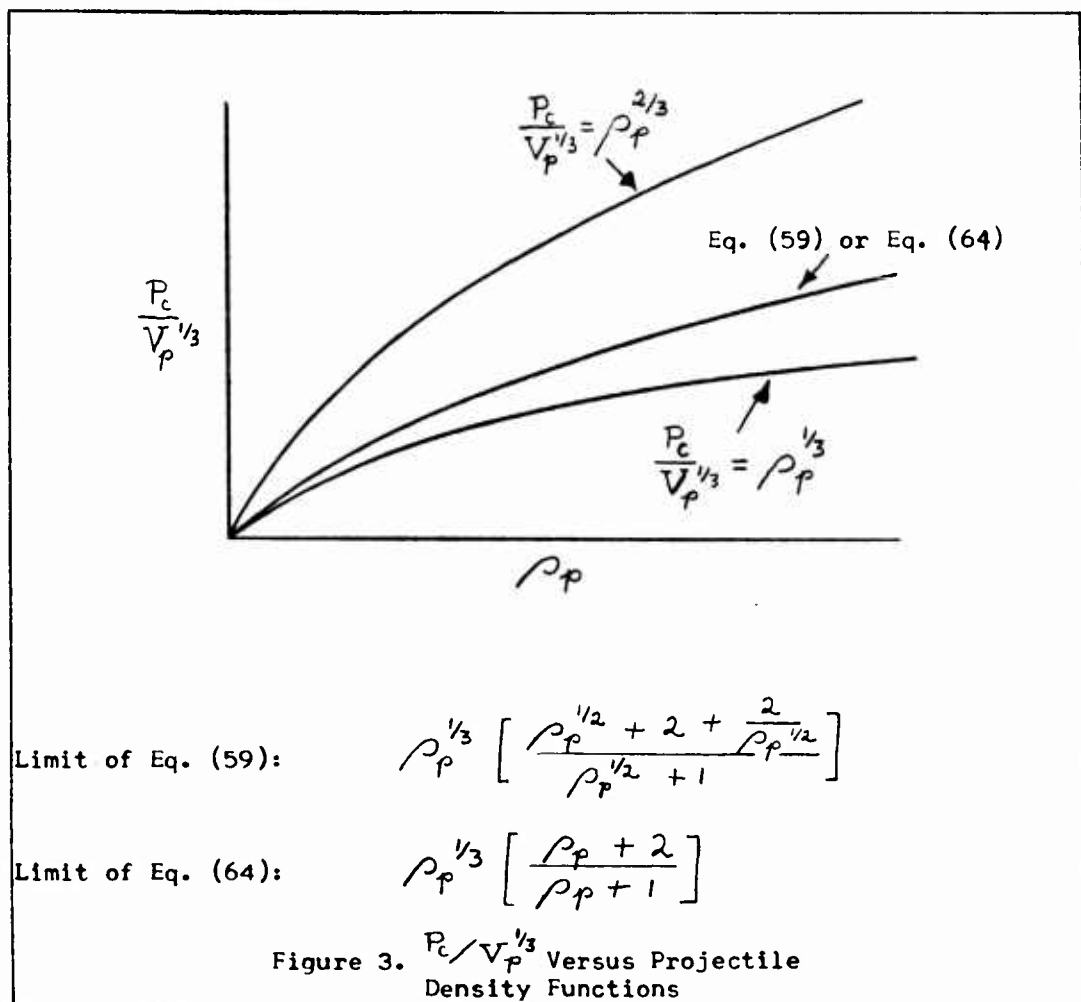
The use of the Bernoulli pressure given by Eq. (10) leads to Eq. (27)

$$\frac{P_c}{V_p^{1/3}} = \frac{\rho_p^{1/3}}{\left[a_3 \frac{1}{K_t} \frac{\rho_p^2 \rho_t^2}{(\sqrt{\rho_p} + \sqrt{\rho_t})^4} v^2 + a_4 (S_g)_t v^{-2} \right]^{1/3}} \qquad (27)$$

If now the shock pressure given by Eq. (19) is used instead of Eq. (10), Eq. (27) becomes

$$\frac{P_c}{V_p^{1/3}} = \frac{\rho_p^{1/3}}{\left[a_3 \frac{1}{K_t} \frac{c_p^2 \rho_p^2 c_t^2 \rho_t^2}{(c_p \rho_p + c_t \rho_t)^2} + a_4 (S_g)_t v^{-2} \right]^{1/3}} \qquad (63)$$

One apparent difference in Eqs. (27) and (63) is the velocity multiplier for the compressibility term only in the case of Eq. (27). This would simply result in a more gradual increase in the compressibility effect relative to the shear toughness effect as impact velocities increase.

Using Eq. (63) instead of Eq. (27), Eqs. (59) and (60) become, respectively

$$\frac{P_c}{V_p^{1/3}} = a \text{ function of } \left[\rho_p^{1/3} + \frac{1}{\rho_p^{2/3}} - \frac{1}{\rho_p^{5/3}} + \frac{1}{\rho_p^{8/3}} - \frac{1}{\rho_p^{11/3}} + \cdots \right] \qquad (64)$$

$$= a \text{ function of } \left[\frac{1}{\rho_t^{2/3}} + \rho_t^{1/3} - \rho_t^{4/3} + \rho_t^{7/3} - \rho_t^{10/3} + \cdots \right] \qquad (65)$$

A comparison of Eqs. (64) and (65) with Eqs. (59) and (60) shows that very similar results are obtained in the penetration expressions, as far as the projectile and target density relationships are concerned. Functions identical to Eq. (65) are obtained for the projectile and target wave

37

velocities, c_p and c_t. It follows that the previous statements regarding the relationship between penetration and target density apply also to projectile and target sonic velocities.

Judging from the previous discussion, an equation of the form of Eqs. (26) or (27) seems to show some promise as a penetration expression for predicting impact behavior over a wide velocity range and for different projectile and target materials. This possibility is being further investigated statistically.

FUTURE WORK

An investigation is being made into possible causes of the low multiple correlation coefficients obtained in the empirical analysis of the high velocity data. Discrepancies in the data can be spotted by calculating the penetration for each individual shot using one or two of the better empirical equations and comparing this with the measured penetration. In this way, the 297 high velocity shots used in the present analysis will be "cleaned up". Further attempts will be made to obtain new high velocity data and thus update the present data.

When an acceptable set of high velocity shots are assembled, this data will be used to check as many existing theories and empirical equations as possible. The data will also be used to test equations developed under the present contract.

Further theoretical work on semi-infinite targets will be confined to minor adjustments of equations already derived in order to better fit the experimental data. It appears likely that the present program will determine, or at least point the way, to an acceptable first order penetration prediction formula for semi-infinite targets.

Unfortunately, the contract time does not permit an analysis of thin targets or oblique impacts. It is hoped, however, that this work may be extended in order to update the present analysis as new, high velocity data appears and in order to extend the study to thin and multiple targets and oblique impacts.

BIBLIOGRAPHY

1. Hayes International Corp., "Study of Target Penetration By High Speed and Ultra High Speed Ballistic Impact - First Quarterly Report", October 31, 1961.

2. Hayes International Corp., "Study of Target Penetration Prediction By High Speed and Ultra High Speed Ballistic Impact - Second Quarterly Report", APGC-TDR-62-11, Feb. 1962.

3. Hayes International Corp., "Study of Target Penetration Prediction By High Speed and Ultra High Speed Ballistic Impact - Third Quarterly Report", April 1962.

4. Hopkins and Kolsky, "Mechanics of Hypervelocity Impact of Solids", Hypervelocity Impact - Fourth Symposium, Vol. 1 (1960) paper #12.

5. Herrmann and Jones, "Survey of Hypervelocity Impact Information", M.I.T. - A.S.R.L. Report No. 99-1, September 1961.

6. Palmer, E. P., "Penetration and Cratering", University of Utah Technical Report UU7, October 13, 1961.

7. Johnson, Cannon, Palmer and Grow, "Cratering Produced in Metals by High-Velocity Impact", University of Utah Technical Report UU4, July 31, 1959.

8. American Institute of Physics Handbook, McGraw Hill Book Company, New York, 1957.

9. Kent, William, Kent's Mechanical Engineers' Handbook, John Wiley and Sons, New York, 1956.

10. Nadai, A., Theory of Flow and Fracture of Solids, McGraw Hill Book Company, New York, 1950.

11. Rinehart, J. S., and Pearson, J., Behavior of Metals Under Impulsive Loads, American Society for Metals, Cleveland, Ohio, 1954.

12. Metals Handbook, The American Society for Metals, Novelty, Ohio, 1948.

13. Military Handbook, MIL-HDBK-5, "Strength of Metal Aircraft Elements", Armed Forces Supply Support Center, Washington, D.C., March 1959.

INITIAL DISTRIBUTION

2	Wpns Sys Eval Gp	2	Nav Wpns Lab (Tech Lib)	
2	Hq USAF (AFDAP/W-AD)	2	Ames Rsch Ctr (Lib)	
2	Hq USAF (ARDRD-ER-1)	2	Ames Rsch Ctr (HSR Div)	
2	ASD (ASRCEP-1)	2	Lewis Rsch Ctr	
2	ASD (ASRCPR-1)	2	Applied Rsch Lab (JHU)	
2	ASD (ASRNGW)	1	Armour Rsch Foundation	
2	AFSWC	1	Franklin Institute (Lib)	
2	OAR	1	Franklin Institute	
2	OAR (RROSA)	1	Jet Propulsion Lab	
2	BSD	1	USAF Proj RAND	
2	SSD	1	University of Chicago (Lib)	
1	AFCRL	15	ASTIA (TIPCR)	
2	AU (AUL-9764)		APGC	
1	TAC (TPL-RQD-M)		ASQR	2
2	Langley Rsch Ctr (Lib)		PGAPI	2
2	Springfield Armory (R&D Div)		PGEH	3
2	Watervliet Arsenal (ORDBR-R)		PGWR	2
2	ARO (Scientific Info Br)		PGW	2
2	ABMA (ORDAB-HT)		PGWRT	40
2	Watertown Arsenal			
2	Picatinny Arsenal (ORDBB-TH8)			
1	BRL (Free-Flight Aero Br)			
1	BRL (Exter Ballistics Lab)			
1	BRL (Tech Info Br)			
1	BRL (Dev & Proff Svcs)			
1	ARGMA (ORDDW-IDE)'			
1	Frankford Arsenal (Lib)			
1	Frankford Arsenal (Pitman-Dunn Lab)			
1	Rock Island Arsenal			
1	CofOrd (ORDTB)			
1	CofOrd (ORDTM)			
1	CofOrd (ORDTS)			
2	NOTS (Code 5007)			
2	NOTS (Tech Lib)			
1	BUWEPS (R-12)			
3	BUWEPS (RM)			
1	BUWEPS (RM-3)			
1	BUWEPS (RMGA-41)			
1	BUWEPS (RT-1)			
1	BUWEPS (RMMO)			
1	NOL (Assoc Dir/Aeroballistics)			
1	NOL (Aerodynamics Dept)			
1	NOL (Ballistics Dept)			
2	NASA (Code 9262)			

Air Proving Ground Center, Eglin Air Force Base, Florida
Rpt No. APGC-TDR-62-51. STUDY OF TARGET PENETRATION
PREDICITON BY HIGH SPEED AND ULTRA HIGH SPEED BALLISTIC
IMPACT. Final report, Sep 1962, 40p. incl tables, 13 refs.
Unclassified Report

A statistical analysis of the penetration depth in semi-infinite targets divided by the diameter of the projectile (P_c/D_p) on 1272 experimental shots has been completed. This data were split into 985 low velocity shots and 297 high velocity shots according to the bulk wave velocity in the target material. Separate analyses of the two groups show interesting relationships with existing theoretical and empirical equations. A semi-rational penetration expression has been developed from a working energy consideration which suggests that the nonrecoverable target compression and shear strain energies may account for most of the kinetic energy of the projectile. Judging from a preliminary comparison with existing experimental data, a penetration model of the form developed herein shows some promise for predicting impact behavior over a wide velocity range and for different projectile and target materials.

1. Hypervelocity projectiles
2. Penetration
3. Digital computers
4. Cratering
I. AFSC Project 9860
II. Contract AF 08(635)-2155
III. Hayes International Corp., Birmingham, Ala.
IV. In ASTIA collection

Air Proving Ground Center, Eglin Air Force Base, Florida
Rpt No. APGC-TDR-62-51. STUDY OF TARGET PENETRATION
PREDICTION BY HIGH SPEED AND ULTRA HIGH SPEED BALLISTIC
IMPACT. Final report, Sep 1962, 40p. incl tables, 13 refs.
Unclassified Report

A statistical analysis of the penetration depth in semi-infinite targets divided by the diameter of the projectile (P_c/D_p) on 1272 experimental shots has been completed. This data were split into 985 low velocity shots and 297 high velocity shots according to the bulk wave velocity in the target material. Separate analyses of the two groups show interesting relationships with existing theoretical and empirical equations. A semi-rational penetration expression has been developed from a working consideration which suggests that the nonrecoverable target compression and shear strain energies may account for most of the kinetic energy of the projectile. Judging from a preliminary comparison with existing experimental data, a penetration model of the form developed herein shows some promise for predicting impact behavior over a wide velocity range and for different projectile and target materials.